Journal of Sound and Vibration (2002) **252**(5), 791–815
doi:10.1006/jsvi.2000.3534, available online at http://www.idealibrary.com on IDEAL®

PERFORMANCE AND DYNAMIC STABILITY OF GENERAL-PATH CENTRIFUGAL PENDULUM VIBRATION ABSORBERS

A. S. Alsuwaiyan and S. W. Shaw

Department of Mechanical Engineering, Michigan State University, East Lansing, MI 48824, *U.S.A.*

(*Received* 10 *June* 1999, *and in final form* 28 *November* 2000)

Centrifugal pendulum vibration absorbers are a type of tuned dynamic absorber used for the attenuation of torsional vibrations in rotating and reciprocating machines. They consist of masses that are constrained to move along specific paths relative to the rotational axis of the machine. Previous analytical studies have considered the performance of single absorber systems with general paths and of multi-absorber systems with a specific path type. In this paper, we investigate the performance and dynamic stability of systems comprised of multiple, identical centrifugal pendulum vibration absorbers riding on quite general paths. The study is carried out by considering a scaling of the system parameters, based on physically realistic ranges of dimensionless parameters, which permits application of the method of averaging. It is found that the performance of these systems is limited by two distinct types of instabilities. In one type, the system of absorbers lose their synchronous character, while in the other a classical non-linear jump affects all absorbers identically, leading to highly undesirable system behavior. These results are used to evaluate two common types of absorber paths, namely circles and cycloids, including intentional mistuning of the absorber frequencies. The results are used to make some recommendations about the selection of paths to achieve design goals in terms of absorber performance and operating range. The analytical predictions are confirmed by numerical simulations.

1. INTRODUCTION

Rotating machines are often subjected to fluctuating torsional loads that can cause noise and vibration difficulties, for example, gear rattle and fatigue failure. Many methods are used to reduce torsional vibrations, including the addition of flywheels [1] and tuned vibration dampers [2–4]. These methods, however, have some shortcomings. Flywheels increase the system inertia, which reduces system responsiveness, while torsional dampers dissipate energy and work at only a single frequency (or a small set of resonant frequencies). Another effective method for reducing torsional vibrations is the use of centrifugal pendulum vibration absorbers (CPVAs). These are masses mounted on the rotor in such a manner that they are free to move relative to it along prescribed paths, and whose motions are used to counteract the applied fluctuating torque, thereby reducing torsional vibration of the rotor. Figure 1 shows a schematic view of an arrangement of CPVAs. The path along which each absorber mass moves is designed to achieve the desired goal.

CPVAs were used in IC engines as early as 1929 [5]. They have been effectively employed to reduce torsional vibrations in light aircraft engines [3], helicopter rotors [6], and automotive racing engines [7]. Until around 1980 all CPVA designs employed simple

0022-460X/02/$35.00

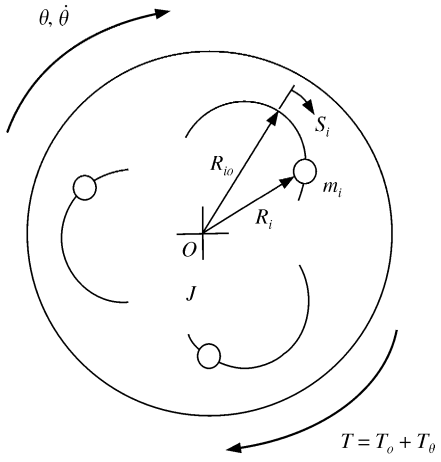

Figure 1. Schematic view of CPVAs mounted on a rotor.

circular paths for the absorbers. These circular paths work fine at small amplitudes, but the non-linear, amplitude-dependent frequency of these simple pendulums limit their effectiveness, and must be accounted for by intentionally mistuning the linearized frequency of the absorber. More recently, other paths that offer improved performance at large amplitudes have been introduced. Cycloidal path absorbers are used in helicopter rotors [6], and epicycloidal path absorbers were proposed for use in automotive engines [8–10]. This epicycloidal path is very special, since it is the path that maintains a constant frequency for the absorber over all amplitudes, thereby keeping the absorbers as linear as possible over a large operating range [8]. This path separates two basic types of paths that are considered in the present study. Paths such as circles exhibit softening non-linear behavior, that is, their frequency of oscillation decreases as the amplitude increases, which leads to many shortcomings in absorber performance. Paths such as cycloids exhibit hardening non-linear behavior in which the frequency of oscillation increases as the amplitude increases and avoid many of the difficulties encountered with circular paths.

Lee and Shaw [11] investigated the performance of a single-mass CPVA for the case of perfectly tuned absorber paths with general non-linear form. They confirmed the shortcomings of circular paths and demonstrated the improvements offered by cycloidal and epicycloidal paths. Shaw *et al.* [12] extended these results to include mistuning of the absorber frequency relative to the applied torque, in addition to a general non-linear nature of the path. They confirmed that overtuning the circular path absorbers significantly improved their operating range, but at the expense of performance. Chao *et al.* [13] investigated the stability of the unison motion for multiple CPVAs riding on perfectly tuned epicycloidal paths.

This paper considers systems of multiple, identical CPVAs riding on mistuned paths with general non-linear form. This includes as special cases those of practical interest, namely, mistuned circular paths, and tuned cycloidal paths. The main objectives of this study are to:

- investigate the stability of the desired unison response in which all absorbers move in a synchronous manner.
- investigate the effects of path parameters, namely mistuning and non-linearity, on the performance of the CPVA system.
- provide some guidelines for use by designers for choosing a path to meet certain goals.

The paper is organized as follows. We begin with a formulation of the equations of motion and a scaling of the system parameters and variables that brings out the features of interest. The resulting equations are studied via the application of averaging, which offers good approximations for the steady state response of the absorbers and the rotor, including stability information. The averaged equations are used to determine specific response features of interest, from which some general observations are made. Simulation results are presented for some case studies, and the paper is closed with a summary and some conclusions.

2. MATHEMATICAL FORMULATION

2.1. EQUATIONS OF MOTION

We consider a system of N CPVAs mounted on a rotor of inertia J, as shown in Figure 1. The equations of motion for the ith absorber and the rotor, respectively, are given by [10]

$$m_i\left[\ddot{S}_i + \tilde{G}_i(S_i)\ddot{\theta} - \frac{1}{2}\frac{\mathrm{d}X_i}{\mathrm{d}S_i}(S_i)\dot{\theta}^2\right] = -c_{ai}\dot{S}_i, \quad i = 1, \ldots, N, \tag{1}$$

$$J\ddot{\theta} + \sum_{i=1}^{N} m_i\left[\frac{\mathrm{d}X_i}{\mathrm{d}S_i}(S_i)\dot{S}_i\dot{\theta} + X_i(S_i)\ddot{\theta} + \tilde{G}_i(S_i)\ddot{S}_i + \frac{\mathrm{d}\tilde{G}_i}{\mathrm{d}S_i}(S_i)\dot{S}_i^2\right]$$
$$= \sum_{i=1}^{N} c_{ai}\tilde{G}_i(S_i)\dot{S}_i - c_0\dot{\theta} + T_0 + T(\theta), \tag{2}$$

where terms are defined as follows. The ith absorber, which has a mass of m_i, is riding on a path specified by the function $R_i(\mathrm{S}_i)$. R_i denotes the distance from a point on the ith absorber path to the center of the rotor, and S_i is an arc length variable along that path, which is used as the generalized co-ordinate for the ith absorber mass. R_{i0} is the value of R_i at the vertex of the path, i.e., $R_{i0} = R_i(0)$. θ represents the angular orientation of the rotor. c_{ai} and c_0 represent the equivalent viscous damping coefficients for the ith absorber and the rotor respectively. T_0 and $T(\theta)$ are the mean and fluctuating components of the applied torque. Note that $T(\theta)$ is periodic in θ with period $2\pi/n$, where n is the minimum order of the torsional excitation. The functions $X_i(S_i)$ and $\tilde{G}_i(X_i)$ are based on the path and are defined as follows:

$$X_i(S_i) = R_i^2(S_i), \qquad \tilde{G}_i(S_i) = \sqrt{X_i(S_i) - \frac{1}{4}\left(\frac{\mathrm{d}X_i}{\mathrm{d}S_i}(S_i)\right)^2}. \tag{3}$$

Equation (1) is the force balance on the ith absorber, and it is important to note that each absorber is indirectly coupled to all the other absorbers through the dynamics of the rotor. Equation (2) represents the torque balance on the rotor, which is affected by each absorber through inertial and damping terms. The general goal of a CPVA system is to find a path such that the resulting dynamics have the absorbers moving in such a manner that they provide a torque on the rotor that cancels, or partially cancels, the fluctuating component of the applied torque.

These equations of motion represent an autonomous dynamical system, because the varying component of the applied torque, $T(\theta)$, is expressed as a function of the rotor angle θ. For purposes of subsequent analysis, it is convenient to choose the rotor angle as the independent variable, replacing time [8]. To this end, and to non-dimensionalize

the problem, we first define a new variable v as the ratio of the rotor angular velocity to the average rotor angular velocity Ω, i.e.,

$$v \equiv \dot{\theta}/\Omega . \tag{4}$$

This dynamic variable will be used to represent rotor speed. It and the S_i's will be the generalized co-ordinates for the system, and these will be functions of θ. Using the chain rule, one can obtain the following relationships between derivatives with respect to time and derivatives with respect to θ:

$$\begin{aligned}
\ddot{\theta} &= \frac{\mathrm{d}^2\theta}{\mathrm{d}t^2} = \Omega^2 v \frac{\mathrm{d}v}{\mathrm{d}\theta} = \Omega^2 v v', \\
(\dot{.}) &= \frac{\mathrm{d}(.)}{\mathrm{d}t} = \Omega v \frac{\mathrm{d}(.)}{\mathrm{d}\theta} = \Omega v (.)', \\
(\ddot{.}) &= \frac{\mathrm{d}^2(.)}{\mathrm{d}t^2} = \Omega^2 v \frac{\mathrm{d}v}{\mathrm{d}\theta}\frac{\mathrm{d}(.)}{\mathrm{d}\theta} + \Omega^2 v^2 \frac{\mathrm{d}^2(.)}{\mathrm{d}\theta^2} \\
&= \Omega^2 v v' (.)' + \Omega^2 v^2 (.)''.
\end{aligned} \tag{5}$$

After equations (1, 2) are non-dimensionalized, and the independent variable is changed from t to θ, the equations of motion become

$$v s_i'' + [s_i' + \bar{g}_i(s_i)]v' - \frac{1}{2}\frac{\mathrm{d}x_i(s_i)}{\mathrm{d}s_i} v = -\mu_{ai} s_i', \quad i = 1, \ldots, N, \tag{6}$$

$$\sum_{i=1}^{N} b_i \left[\frac{\mathrm{d}x_i(s_i)}{\mathrm{d}s_i} s_i' v^2 + x_i(s_i) v v' + \tilde{g}_i(s_i) s_i' v v' + \tilde{g}_i(s_i) s_i'' v^2 + \frac{\mathrm{d}\tilde{g}_i(s_i)}{\mathrm{d}s_i} s_i^2 v^2 \right] + v v'$$

$$= \sum_{i=1}^{N} b_i \mu_{ai} \tilde{g}_i(s_i) s_i' v - \mu_0 v + \Gamma_0 + \Gamma(\theta), \tag{7}$$

where

$$\begin{aligned}
s_i &= S_i/R_{i0}, \quad b_i = I_i/J, \\
I_i &= m_i R_{i0}^2, \quad \mu_{ai} = c_{ai}/m_i\Omega, \quad \mu_0 = c_0/J\Omega, \\
\Gamma_0 &= T_0/J\Omega^2, \quad \Gamma(\theta) = T(\theta)/J\Omega^2
\end{aligned}$$

and

$$\begin{aligned}
x_i(s_i) &= X_i(s_i R_{i0})/R_{i0}^2, \\
\tilde{g}_i(s_i) &= \sqrt{x_i(s_i) - \frac{1}{4}\left(\frac{\mathrm{d}x_i}{\mathrm{d}s_i}(s_i)\right)^2}.
\end{aligned} \tag{8}$$

Note that the system is now non-autonomous, but its degree has been reduced, since only first derivatives in v appear. Assuming that all the absorbers have the same mass, and all

paths have the same value of R_i at each vertex, i.e., $m_i = m$, $R_{i0} = R_0 \,\forall i \in [1,\ N]$, equation (7) becomes

$$\frac{b_0}{N}\sum_{i=1}^{N}\left[\frac{\mathrm{d}x_i(s_i)}{\mathrm{d}s_i}s_i' v^2 + x_i(s_i)vv' + \tilde{g}_i(s_i)s_i' vv' + \tilde{g}_i(s_i)s_i'' v^2 + \frac{\mathrm{d}\tilde{g}_i(s_i)}{\mathrm{d}s_i}s_i^2 v^2\right] + vv'$$

$$= \frac{b_0}{N}\sum_{i=1}^{N}\mu_{ai}\tilde{g}_i(s_i)s_i' v - \mu_0 v + \Gamma_0 + \Gamma(\theta), \tag{9}$$

where $b_0 = I_0/J$, $I_0 = m_0 R_0^2$, and $m_0 = Nm$.

The fluctuating torque generally contains several harmonics. In most situations, only one or two harmonics have significant amplitude, and therefore we approximate the fluctuating torque by its dominant harmonic, taken to be of order n, as follows: $\Gamma(\theta) = \Gamma_\theta \sin(n\theta)$. For example, in four-stroke internal combustion engines, n is equal to half the number of cylinders.

2.2. GENERAL PATH REPRESENTATION

In the present study, a two-parameter family of paths is considered. The designer can select these two parameters in order to achieve certain goals in terms of absorber performance. As described by Denman [8], it is convenient to represent the path for the ith absorber by the local radius of curvature at any point on the path, given by

$$\rho_i = \sqrt{\rho_{i0}^2 - \lambda^2 S_i^2}.$$

Here ρ_{i0} is the path's radius of curvature at the vertex, which dictates the small amplitude nature of the path. The parameter λ dictates the large amplitude character of the path, and typically takes on values from zero to one.

The order of the path $\tilde{n}_i$ is given by the square root of the ratio of the distance from the rotor center to the center of the path vertex circle and the path vertex radius of curvature [8], that is,

$$\tilde{n}_i = \sqrt{\frac{R_{i0} - \rho_{i0}}{\rho_{i0}}}. \tag{10}$$

This fixes the small amplitude (linearized) natural frequency of the ith absorber, when the rotor spins at a constant rate Ω, to be $\tilde{n}_i\Omega$. This frequency is used for tuning the absorber at small amplitudes. It is a central feature of these absorbers that this frequency is proportional to the mean rotation rate, Ω, since this allows the absorber to remain tuned to a given order at all rotation speeds of the machine. Based on purely linear considerations, the order of the path for a CPVA should be tuned to the frequency of the disturbance torque, that is, $\tilde{n}_i = n$. In the linear, undamped case this makes the absorber perfectly effective, since the rotor vibrations are completely eliminated. However, the non-linear effects that arise from the frequency–amplitude dependence of the absorber can be handled by incorporating a small level of intentional linear mistuning on the path, a technique implemented in practice [14].

The value of λ dictates the nature of the amplitude-dependent frequency of the absorber when it oscillates freely along its path. Some special cases of interest are: $\lambda = 0$ describes a circular path, $\lambda = \lambda_e = \sqrt{\tilde{n}_i^2/(\tilde{n}_i^2 + 1)}$ describes an epicycloidal path with its base circle of

radius ($R_{i0} - \rho_{i0}$) centered at the rotor center (this is the tautochronic path of order $\tilde{n}_i$ [8]), and $\lambda = 1$ describes a cycloidal path.

In the equations of motion an expression for $x_i(s_i)$ for the general absorber path is needed (see equations (6, 9)). The following expression can be obtained by expanding in s_i,

$$x_i(s_i) = 1 - \tilde{n}_i s_i^2 + \gamma_i s_i^4 + \mathrm{O}(s_i^6), \tag{11}$$

where

$$\gamma_i = (\tfrac{1}{12})(\tilde{n}_i^2 + 1)^3(\lambda_e^2 - \lambda^2).$$

Here the function $x_i(s_i)$ can be thought of as a type of potential function, where the quadratic term dictates the linear system behavior (frequency) and the quartic term determines the non-linear behavior (the frequency–amplitude dependence). It is clear from this that softening paths (such as the circle, $\lambda = 0$) correspond to positive values of γ_i, while hardening paths (such as the cycloid, $\lambda = 1$) correspond to negative values of γ_i. And $\gamma_i = 0$ represents the tautochronic epicycloidal path, which is neither softening nor hardening.

Note that the expanded forms of x_i and g_i are used in the analysis, but their full forms are used in the numerical simulations.

2.3. SCALING

Since the ratio of the total absorbers' inertia, I_0, to the rotor inertia, J, is small, we define a small parameter ε as

$$\varepsilon^p = b_0.$$

The parameter ε forms the basis used for the scaling. The value of p, and other similar scaling powers, will be determined later, and are selected such that the non-linear analysis captures the desired information. Note that in the unperturbed case, $\varepsilon = 0$, the rotor dynamically de-couples from the absorbers, since the absorbers have zero inertia.

To account for the mistuning between the absorber and the applied torque, the path order is expressed by

$$\tilde{n}_i = n(1 + \varepsilon^q \sigma_i), \tag{12}$$

where σ_i represents a measure of the mistuning of the ith absorber path and q is to be determined. Such mistuning is essential for the satisfactory performance of circular path absorbers [14].

The preferred absorber configuration has small damping, since it remains tuned relative to the disturbance at all rotational speeds. In addition, the fluctuating torque amplitude is small compared to the kinetic energy of the rotor, rendering the non-dimensional torque amplitude small. Therefore, the parameters μ_a, μ_0, Γ_0, and Γ_θ can be taken to be small and are scaled by ε as follows:

$$\mu_a = \varepsilon^l \tilde{\mu}_a, \quad \mu_0 = \varepsilon^l \tilde{\mu}_0, \quad \Gamma_0 = \varepsilon^l \tilde{\Gamma}_0, \quad \Gamma_\theta = \varepsilon^r \tilde{\Gamma}_\theta,$$

where the powers l and r are to be determined. In addition, the amplitude of the absorber oscillations are assumed to scale with the fluctuating torque level in some manner, and so we take

$$s_i = \varepsilon^v z_i, \tag{13}$$

where v is to be determined.

We now turn to the matter of balancing the desired terms in the equations of motion so that the applied torque, the damping, and the non-linearities come into play in the same order. We begin with a couple of preliminary expansions.

Note that when $\varepsilon = 0$, i.e., $b_0 = 0$, $\mu_0 = 0$, $\mu_a = 0$, $\Gamma_0 = 0$, and $\Gamma_\theta = 0$, equation (9) yields $vv' = 0$, which implies that the rotor spins at a constant angular speed. This speed has been denoted as Ω, so that the corresponding non-dimensional rotor speed is given by $v = 1$. For $0 < \varepsilon \ll 1$, the rotor will have small fluctuations about this constant angular speed, and it is convenient to expand the rotor speed as

$$v(\theta) = 1 + \varepsilon^w v_w(\theta) + HOT, \tag{14}$$

where w is to be determined.

The path functions can be expanded in terms of ε as well. Evaluating $\tilde{g}_i$ and x_i using equations (8), (11), (12), and (13), and expanding them in powers of ε, the following expressions can be obtained:

$$\tilde{g}_i(z_i) = 1 - \varepsilon^{2v} \frac{(n^2 + n^4)z_i^2}{2} + HOT, \tag{15}$$

$$\gamma_i = \gamma_0 + \mathrm{O}(\varepsilon^q),$$

where

$$\gamma_0 = (\tfrac{1}{12})(n^2 + 1)^3(\lambda_{e0}^2 - \lambda^2), \tag{16}$$

where $\lambda_{e0} = n^2/(1 + n^2)$. Note that for $\gamma_0 > 0$ ($\lambda_{e0} > \lambda$) the absorber non-linearity is softening, that is, its frequency decreases as a function of amplitude, whereas for $\gamma_0 < 0$ ($\lambda_{e0} < \lambda$), the absorber non-linearity is hardening, that is, its frequency increases as a function of amplitude. The case $\gamma_0 = 0$ ($\lambda_{e0} = \lambda$) is precisely the tautochronic epicycloid [8].

The final preliminary step is to note that in order for the constant torque terms to balance, $\Gamma_0 = \mu_0$ must hold. This is the non-dimensional form of $T_0 = c_0\Omega$, which states that the net constant applied torque (including any constant load) is resisted by the average bearing resistance to set the mean rotation rate.

Substituting the above scaled parameters, the constant torque balance, the expressions for $\tilde{g}_i(s_i)$, γ_i, and $v(\theta)$ into equation (9), then expanding, setting $r = (p + v)$ and keeping the ε^r and ε^{r+v} order terms, one finds that the non-dimensional rotor acceleration is given by

$$vv'(\theta) = \varepsilon^r \left\{ \frac{1}{N} \sum_{j=1}^{N} n^2 z_j + \tilde{\Gamma}_\theta \sin(n\theta) \right\} + \frac{\varepsilon^{r+v}}{N} \sum_{j=1}^{N} 2n^2 z_j z_j' + HOT. \tag{17}$$

Here the leading term is that predicted by the linear theory, and is composed of the reaction to the applied torque and the restoring forces from the absorbers. The second term is the first non-linear correction, which arises from Coriolis effects of the absorbers' motions.

Using this result in equation (6), and expanding using all the information developed to this point, a suitable choice of the scaling orders is found to be

$$q = 1, \quad v = \tfrac{1}{2}, \quad l = 1, \quad r = \tfrac{3}{2}, \quad p = 1, \quad w = \tfrac{3}{2}.$$

This leads to the desired form of the absorber equations, in which the effects of the applied torques, damping, and non-linearity are captured in the first non-linear correction.

2.4. THE AVERAGED EQUATIONS

With the above scaling results, the rotor dynamics can be eliminated to leading order from the absorber dynamics. This is done by substituting the expansions from equations (11), (15), and (17) into equation (6), and expanding using the scaling assumptions and conditions outlined above. This results in the following equations that describe the dynamics of the absorbers:

$$z_i'' + n^2 z_i = \varepsilon\left[2\gamma_0 z_i^3 - 2n^2\sigma_i z_i - \tilde{\mu}_a z_i' - \frac{n^2}{N}\sum_{j=1}^{N} z_j - \tilde{\Gamma}_\theta \sin(n\theta)\right] + HOT. \tag{18}$$

These equations contain the effects of the rotor dynamics on the absorbers to the order retained. They are expressed in terms of the applied torque and the torques from all absorbers acting on the rotor, which are contained in the summation term.

It should be noted here that at the order considered, the only non-linear effect that appears is the one due to the path, i.e., $\gamma_0 z_i^3$. Missing at this order are all of the non-linear terms that arise from the kinematic coupling of the rotation and the absorber motion. The non-linear path term is zero for epicycloidal paths because $\gamma_0 = 0$ (cf. equation (16)). In this case, the model reduces to the linearized one, with which it is impossible to capture any non-linear effects. Therefore, in order to analyze the case of epicycloidal paths, one has to employ a scaling wherein non-linearities other than the path non-linearity are retained. Chao *et al.* [13] have done this and analyzed the case of perfectly tuned epicycloidal paths in some detail. In the present study, epicycloidal paths are not considered.

Equation (18) is weakly non-linear, due to the amplitude scaling, and weakly coupled, due to the small inertia of the absorbers relative to the rotor. It shows that the system of absorbers has some very special dynamical features, including the facts that each absorber has an identical unperturbed natural frequency, and each absorber is resonantly excited by the fluctuating applied torque. Furthermore, the absorbers are all coupled to one another in exactly the same manner. When they are identical in mass, path, and damping, the system possesses a special symmetry that can be used to exploit the analysis of the system dynamics (see references [13, 15]).

The averaging method will be used to determine approximate steady state solutions of these equations. To obtain the standard periodic form, the usual transformation to polar (amplitude and phase) co-ordinates is used,

$$z_i = a_i \sin(n\theta + \phi_i), \qquad z_i' = n a_i \cos(n\theta + \phi_i). \tag{19}$$

The standard period form for the equations is found to be

$$a_i' = \frac{\varepsilon}{n} f_i \cos(n\theta + \phi_i) + HOT, \qquad \phi_i' = -\frac{\varepsilon}{n a_i} f_i \sin(n\theta + \phi_i) + HOT, \tag{20}$$

where

$$\begin{aligned} f_i = {} & 2\gamma_0 a_i^3 \sin^3(n\theta + \phi_i) - 2n^2\sigma_i a_i \sin(n\theta + \phi_i) \\ & - \tilde{\mu}_a n a_i \cos(n\theta + \phi_i) - \frac{n^2}{N}\sum_{j=1}^{N} a_j \sin(n\theta + \phi_j) \\ & - \tilde{\Gamma}_\theta \sin(n\theta). \end{aligned} \tag{21}$$

The functions f_i are periodic in the independent variable θ, with period $(2\pi/n)$. Averaging these equations over one period, one reaches the following averaged equations:

$$\bar{a}_i' = \varepsilon\left[-\frac{\tilde{\mu}_a}{2}\,\bar{a}_i + \frac{\tilde{\Gamma}_\theta}{2n}\sin(\bar{\phi}_i) + \frac{n}{2N}\sum_{j=1,\,j\neq i}^{N}\bar{a}_j\sin(\bar{\phi}_i - \bar{\phi}_j)\right] + HOT,$$

$$\bar{a}_i\bar{\phi}_i' = \varepsilon\left[-\frac{3\gamma_0}{4n}\,\bar{a}_i^3 + n\left(\sigma_i + \frac{1}{2N}\right)\bar{a}_i + \frac{\tilde{\Gamma}_\theta}{2n}\cos(\bar{\phi}_i)\right] + \frac{n}{2N}\sum_{j=1,\,j\neq i}^{N}\bar{a}_j\cos(\bar{\phi}_i - \bar{\phi}_j) + HOT, \tag{22}$$

where an overbar indicates the averaged value of the corresponding variable. These equations are the basis of the analysis of the system dynamics.

2.5. EXISTENCE AND STABILITY OF UNISON RESPONSE

In this section, we consider the case in which all absorbers are identical and move in a perfectly unison (synchronous) manner. This is the desired response of the absorbers, so its existence and stability are of interest.

One objective of this study is to determine the effects of intentional linear mistuning, and so we fix an identical level of mistuning for all absorber paths, as follows:

$$\sigma_i = \sigma \quad \forall i \in [1, N].$$

For a unison response all absorbers have the same vibration amplitude and phase, i.e.,

$$\bar{a}_i = r_z, \quad \bar{\phi}_i = \phi_z \quad \forall i.$$

When these are substituted into equation (22), they become pairwise identical and reduce to

$$r_z' = \varepsilon\left[-\frac{\bar{\mu}_a}{2}\,r_z + \frac{\tilde{\Gamma}_\theta}{2n}\sin(\phi_z)\right] + HOT,$$

$$r_z\phi_z' = \varepsilon\left[-\frac{3\gamma_0}{4n}\,r_z^3 + n\left(\sigma + \frac{1}{2}\right)r_z + \frac{\tilde{\Gamma}_\theta}{2n}\cos(\phi_z)\right] + HOT.$$

These are nothing more than the averaged equations for the case of a single absorber whose mass is $m_0 = Nm$. The steady state conditions for this unison motion are given by

$$\frac{\mu_a}{2}\,r_z = \frac{\tilde{\Gamma}_\theta}{2n}\sin(\phi_z), \tag{23}$$

$$\frac{3\gamma_0}{4n}\,r_z^3 - n\left(\sigma + \frac{1}{2}\right)r_z = \frac{\tilde{\Gamma}_\theta}{2n}\cos(\phi_z). \tag{24}$$

Eliminating the phase in the standard manner, and solving for the torque amplitude in terms of the absorber amplitude (for ease of plotting), one obtains

$$\tilde{\Gamma}_\theta = 2n\sqrt{\left[\frac{\mu_a}{2}\,r_z\right]^2 + \left[\frac{3\gamma_0}{4n}\,r_z^3 - n\left(\sigma + \frac{1}{2}\right)r_z\right]^2}. \tag{25}$$

These results relate in a simple manner the absorber response, in terms of amplitude and phase, to the system path parameters, the damping level, and the fluctuating torque amplitude.

In order to analyze the stability of this unison response, the Jacobian of the system equations (22) must be evaluated at the steady state conditions. This yields a circulant matrix of the form

$$A = \begin{bmatrix} A1 & A2 & . & . & . & A2 \\ A2 & A1 & A2 & . & . & A2 \\ . & . & . & . & . & . \\ A2 & . & . & . & A1 & A2 \\ A2 & . & . & . & . & A1 \end{bmatrix}_{2N\times 2N}, \tag{26}$$

where $A1$ and $A2$ are 2×2 matrices with the following entries:

$$A1_{11} = -\frac{\mu_a}{2}, \qquad A1_{12} = \frac{n}{2N}(N-1)r_z + \frac{\tilde{\Gamma}_\theta}{2n}\cos(\phi_z),$$

$$A1_{21} = -\frac{3\gamma_0}{2n}r_z - \frac{\tilde{\Gamma}_\theta}{2nr_z^2}\cos(\phi_z) - \frac{n(N-1)}{2Nr_z},$$

$$A1_{22} = -\frac{\tilde{\Gamma}_\theta}{2n}\sin(\phi_z), \qquad A2_{11} = 0,$$

$$A2_{12} = -\frac{\mathrm{n}}{2N}r_z, \qquad A2_{21} = \frac{n}{2Nr_z}, \qquad A2_{22} = 0.$$

The block structure of this matrix is not surprising if one considers that the (i, j) 2×2 block represents the effect that perturbations in the steady state motion of absorber i has on absorber j when the entire system is in a synchronous motion.

If all the eigenvalues of the Jacobian matrix have negative real parts, the unison response is asymptotically stable. For a Jacobian of this form it can be shown that each eigenvalue of the 2×2 matrix $[A1 - A2]$ is an eigenvalue of the Jacobian matrix A repeated $(N-1)$ times, and the remaining two eigenvalues are the eigenvalues of the 2×2 matrix $[A1 + (N-1)A2]$ [16]. For the stability evaluation we will use the fact that both eigenvalues of a 2×2 matrix have negative real parts if and only if its determinant is positive and its trace is negative.

When evaluated on the unison response the matrix $[A1 - A2]$ is given by

$$\begin{bmatrix} -\frac{\mu_a}{2} & \frac{3\gamma_0}{4n}r_z^3 - n\sigma r_z \\ \frac{n\sigma}{r_z} - \frac{9\gamma_0}{4n}r_z & -\frac{\mu_a}{2} \end{bmatrix}. \tag{27}$$

Its trace is equal to $-\mu_a$ and is always negative. Its determinant is given by

$$\frac{27\gamma_0^2}{16n^2}r_z^4 - 3\gamma_0\sigma r_z^2 + \left(n^2\sigma^2 + \frac{\tilde{\mu}_a^2}{4}\right). \tag{28}$$

For the unison response the matrix $[A1 + (N-1)A2]$ is given by

$$\begin{bmatrix} -\frac{\mu_a}{2} & \frac{3\gamma_0}{4n} r_z^3 - n\left(\sigma + \frac{1}{2}\right) r_z \\ \left(\sigma + \frac{1}{2}\right)\frac{1}{r_z} - \frac{9\gamma_0}{4n} r_z & -\frac{\mu_a}{2} \end{bmatrix}. \tag{29}$$

Its trace is equal to $-\mu_a$ and its determinant is given by

$$\frac{27\gamma_0^2}{16n^2} r_z^4 - \frac{3}{2}\gamma_0(1 + 2\sigma) r_z^2 + \left[n^2\sigma + n^2\sigma^2 + \frac{1}{4}(n^2 + \mu_a^2)\right]. \tag{30}$$

Since the traces are both negative, no Hopf bifurcations involving complex eigenvalues are possible. This implies that instabilities to quasi-periodic motions, which would represent travelling waves in the absorber system, are not possible. The conditions at which stability changes occur are captured by setting $\mathrm{Det}[A1 - A2] = 0$ and $\mathrm{Det}[A1 + (N-1)A2] = 0$, in which case real eigenvalues pass through the origin in the complex plane. It is quite easy to solve these conditions for the corresponding critical values of the absorber amplitude, yielding values of r_z at which bifurcations occur. The attendant critical torque levels can then be found from equation (25).

It should be noted that solutions of equation (28) represent critical amplitudes at which the unison motion becomes unstable, but continues to exist, resulting in the birth of some type(s) of non-synchronous, steady state response(s). On the other hand, solutions of equation (30) represent conditions at which the unison response is annihilated in a saddle-node bifurcation, representing a sudden jump in the absorbers' motion to another response branch, which may or may not be of unison type. It can be seen that $\mathrm{Det}[A1 + (N-1)A2] = 0$ corresponds to instabilities that preserve the unison nature of the response by considering the stability of the equivalent single-absorber mass system represented by equation (23), and noting that it gives the same instability condition. The other type of instability arises purely from the fact that there are multiple absorbers.

When equations (28, 30) are set equal to zero and solved for r_z, the following results are obtained. For the bifurcation to a non-unison response, $\mathrm{Det}[A1 - A2] = 0$:

$$r_{zbif} = \frac{4n}{\sqrt{6\gamma_0}}\left[\sigma - \left(\sigma^2 - \frac{3}{4n^2}\left(n^2\sigma^2 + \frac{\tilde{\mu}_a^2}{4}\right)\right)^{1/2}\right]^{1/2}. \tag{31}$$

For the jump condition, $\mathrm{Det}[A1 + (N-1)A2] = 0$:

$$r_{zj} \approx \frac{2n}{3}\sqrt{\frac{(\sigma + \frac{1}{2})}{\gamma_0}}, \tag{32}$$

where the approximation is noted because we have neglected the damping term in the torque equation, since it is very small compared to other terms. These can be used in equation (25) to determine the attendant critical torque levels.

The following general observations can be made by considering these two critical conditions.

From the first condition, the bifurcation to non-unison.

- For $\gamma_0 > 0$ (softening non-linear paths, like circles), the bifurcation to non-unison exists only when the level of mistuning is greater than some positive value set by the damping

level and n. (In order to see this observation, the damping term was not neglected in this equation, as was done in the second equation.)
- For $\gamma_0 < 0$ (hardening non-linear paths, like cycloids), the bifurcation to non-unison exists only when the level of mistuning is negative.

From the second condition, the jump bifurcation.

- For $\gamma_0 > 0$ (softening paths), a jump exists only when $\sigma > -\frac{1}{2}$.
- For $\gamma_0 < 0$ (hardening paths), a jump exists only when $\sigma < -\frac{1}{2}$.

It should be noted that in practice one typically overtunes circular path absorbers, that is, $\sigma > 0$, so that the jump is avoided. However, this may promote bifurcations to non-unison, a possibility considered below. Also, it is seen that hardening paths avoid both types of bifurcations simply by taking $\sigma \geqslant 0$.

2.5.1. *Results for two common absorber paths*

2.5.1.1. Circular paths. For circular paths $\lambda = 0$ which, when used in equation (16), gives the following expression for the non-linear path coefficient:

$$\gamma_0 = \tfrac{1}{12} n^2(1 + n^2)^2. \tag{33}$$

When this is substituted into equations (28, 30), the following equations are obtained for the critical stability conditions:

$$\frac{3}{256} n^2(1 + n^2)^4 r_z^4 - \tfrac{1}{4} n^2(1 + n^2)^2 \sigma r_z^2 + \left(n^2\sigma^2 + \frac{\bar{\mu}_a^2}{4} \right) = 0, \tag{34}$$

$$\frac{3}{256} n^2(1 + n^2)^4 r_z^4 - \tfrac{1}{8} n^2(1 + n^2)^2(1 + 2\sigma) r_z^2 + \tfrac{1}{4}[n^2(1 + 2\sigma)^2 + \tilde{\mu}_a^2] = 0, \tag{35}$$

corresponding to the bifurcation to non-unison and the jump conditions respectively.

2.5.1.2. Cycloidal paths. Here $\lambda = 1$ and γ_0 is given by

$$\gamma_0 = -\frac{1}{12}(1 + n^2)^2. \tag{36}$$

When this is substituted into equations (28,30), the following equations are obtained for the critical stability conditions:

$$\frac{3}{256n^2}(1 + n^2)^4 r_z^4 + \tfrac{1}{4}(1 + n^2)^2 \sigma r_z^2 + \left(n^2\sigma^2 + \frac{\bar{\mu}_a^2}{4} \right) = 0, \tag{37}$$

$$\frac{3}{256n^2}(1 + n^2)^4 r_z^4 + \tfrac{1}{8}(1 + n^2)^2(1 + 2\sigma) r_z^2 + \tfrac{1}{4}[n^2(1 + 2\sigma)^2 + \tilde{\mu}_a^2] = 0, \tag{38}$$

corresponding to the bifurcation to non-unison and the jump conditions respectively.

Since these equations are all quadratic in r_z^2, they can be solved to relate the critical absorber amplitude to the tuning order, the mistuning, and the absorber damping level. This can then be substituted into equation (25) to determine the corresponding critical torque levels.

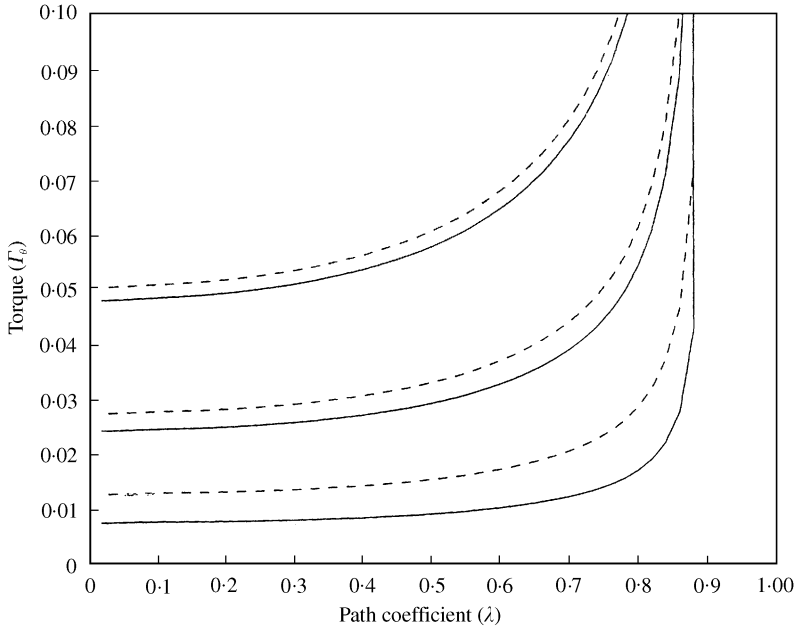

Figure 2. Analytical prediction of the effect of absorber path type and mistuning on bifurcation torque levels. Solid lines are for the bifurcation to non-unison responses, and dashed lines are for the jump bifurcation. The three pairs of lines, moving from lower to upper, are for mistuning levels of 0·5 ($\sigma = 0{\cdot}1$), 2·5 ($\sigma = 0{\cdot}5$), and 5·0% ($\sigma = 1{\cdot}0$).

3. NUMERICAL EXAMPLES AND DISCUSSION

The values of all parameters are fixed for these examples except the two path parameters and the fluctuating torque level. This demonstrates how one would select the path parameters that give effective operation for a given torque order over a range of torque levels. CPVA systems with an inertia ratio of $\varepsilon = 1/20$ are considered, and the order of the applied fluctuating torque is taken to be $n = 2$. The non-dimensional absorber damping coefficient is taken to be $\bar{\mu}_a/N = 0{\cdot}02$, and the dimensionless rotor damping coefficient is taken to be $\mu_0 = 0{\cdot}005$.[†] For numerical simulations, the exact representations of the paths were used, not the expansions in terms of ε that were used in the analysis.

3.1. EFFECT OF PATH TYPE ON BIFURCATIONS

Using the above numerical values in equations (31, 32), along with equation (25), the critical torque levels were obtained as functions of the path coefficient (λ) for various levels of mistuning. The results are presented in Figure 2. It is worth mentioning here that the plot shows only positively mistuned paths ranging from circular up to, but not including, epicycloidal ($0 \leqslant \lambda < \lambda_e$). This is because, as seen in section 2.5, for paths with $\lambda > \lambda_e$, neither bifurcation to non-unison nor jumps are present for positive mistuning levels. Also, as described below, negative mistuning levels are not of practical importance and should always be avoided.

[†] As is typical in many vibration studies, these damping levels are the most elusive of the parameters involved in this study, since they cannot be predicted from first principles.

It is clear from the figure that the dependence of the critical torque levels on the non-linear path parameter is not very significant until one begins to approach the epicycloid. From the stability point of view, no benefits are gained by changing from the easily manufactured circular paths to other paths with $\lambda < \lambda_e$. However, the performance of the absorbers must also be considered before drawing general conclusions.

The level of mistuning does have a significant effect on the stability levels, but, again, performance must be taken into account. Also, note that near the epicycloidal path, that is, for $\lambda \approx \lambda_e = 0{\cdot}89$ the critical torque levels for both bifurcations become large. Here the results are not reliable because, as mentioned earlier, the theory does not work for epicycloidal paths, due to the scaling employed. In both cases—increased mistuning and $\lambda \approx \lambda_e$—the response becomes more like that of a linear system, and thus more stable. In the case of increased mistuning, this is due to the fact that we are moving away from a resonance condition. For $\lambda \approx \lambda_e$, the non-linear part of the path is balanced exactly between softening and hardening; this is the tautochronic condition [8].‡

Our goal is to investigate the operating range of absorber systems, as they are limited by the critical torque levels, and to evaluate the effectiveness of the absorbers by computing the angular acceleration of the rotor, which is desired to be small. We focus on circular and cycloidal absorber paths and distill some general conclusions regarding choices of path parameters.

3.2. CIRCULAR PATHS

We begin by demonstrating the accuracy of the analytical results, and then turn to a more systematic parameter investigation. Figure 3 depicts the unison absorber response versus torque level, showing both theoretical results from equations (34, 35) and numerical simulation results for $N = 4$ absorbers with 0 and 4% mistuning levels. Note that as the absorber amplitudes become larger, for example, on the upper response branches shown in Figure 3, the analytical results become less accurate, due to the amplitude expansions employed. Figure 4(a) shows the critical torque levels above which the unison motion becomes unstable and Figure 4(b) shows the critical torque levels above which the jump occurs, both for different mistuning levels, again for $N = 4$. These results demonstrate the validity of the analytical approach employed.

It can be seen from equation (34) that one can extend the range of the stable unison response by varying the number of absorbers, N. However, the dependence on this parameter is very small. To see this, three different mistuning levels of the paths in the present numerical example are considered. They are 1 ($\sigma = 0{\cdot}2$), 2 ($\sigma = 0{\cdot}4$), and 4% ($\sigma = 0{\cdot}8$). With all other numerical values fixed, increasing the number of absorbers from 2 to 14 in each case increases the critical torque levels at which the bifurcation to non-unison takes place by only 8, 2, and 0·4% respectively. The practical method for extending the range of the stable unison response, as mentioned earlier and as seen from Figure 4(a), is to increase the level of mistuning in the paths. In fact, this will significantly delay both of the bifurcation points.

The response curves for $N = 4$, with different mistuning levels is depicted in Figure 5. This shows that the jump point shifts rightward as the level of mistuning is increased. Figure 5 also shows that as the level of mistuning is increased, the absorbers' amplitudes on the lower branch become smaller for a given torque level, which implies that the absorbers

‡ In previous work it has been shown that the perfectly tuned epicycloidal path exhibits a bifurcation to non-unison, but not a jump [15].

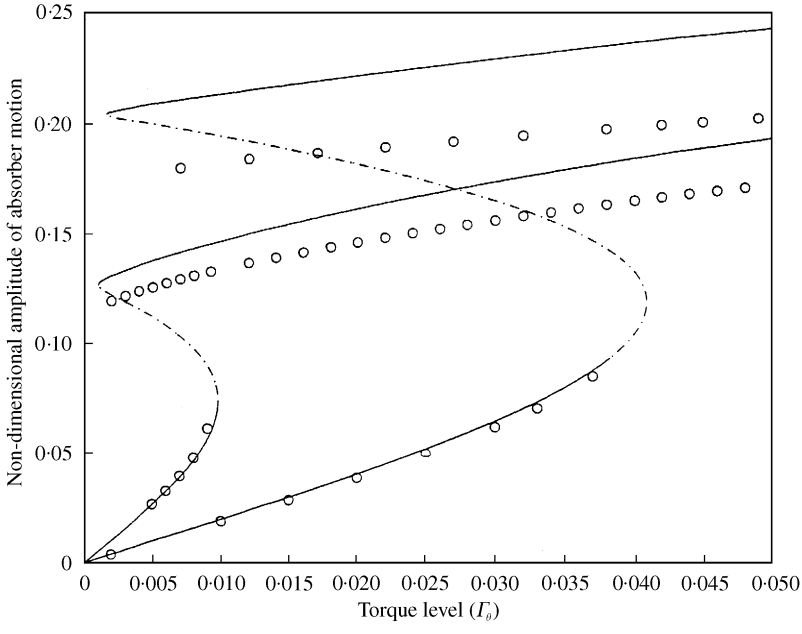

Figure 3. Absorber response amplitude versus torque level for $N = 4$ circular path absorbers with mistuning levels of 0 ($\sigma = 0$) and 4% ($\sigma = 0{\cdot}80$). Curves represent responses predicted by the analysis, with —— lines corresponding to stable responses and – – – lines representing unstable responses. ○ ○ ○ circles indicate results from numerical simulations.

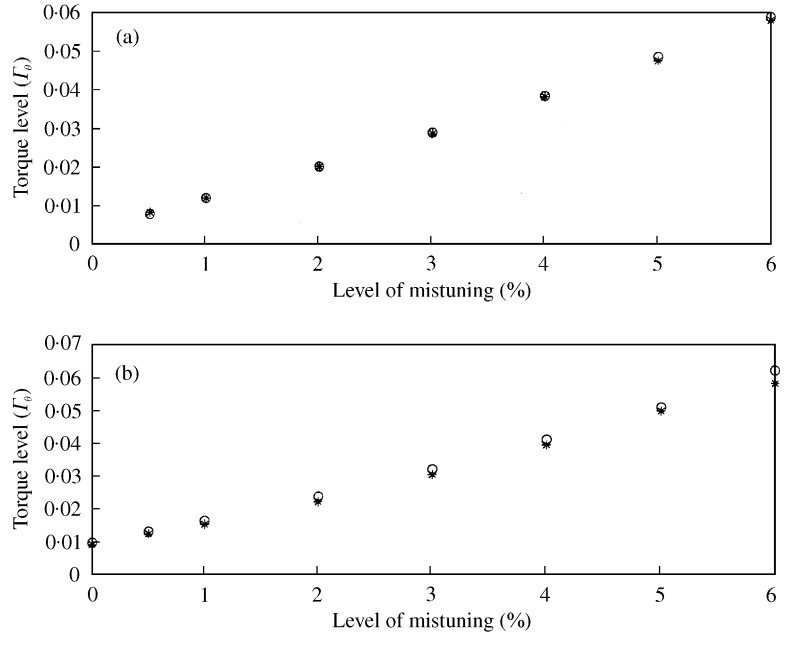

Figure 4. Bifurcation torque levels versus mistuning for circular path CPVAs. ○ ○ ○ circles are the theoretical predictions and "*"'s are results from numerical simulations. (a) Bifurcation to non-unison, (b) Jump.

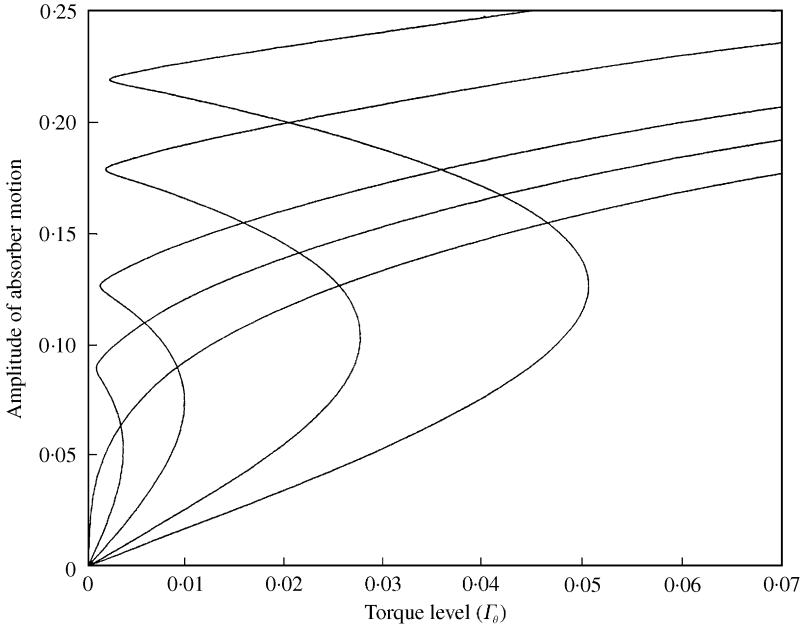

Figure 5. Absorber amplitude versus torque level for several levels of mistuning for circular path CPVAs. Moving from the top curve downward, the mistuning levels are: $\sigma = 1{\cdot}0,\ 0{\cdot}5,\ 0,\ -0{\cdot}25,\ -0{\cdot}5$. Stability is not indicated here.

are cancelling less of the applied torque. This indicates that there is a tradeoff between large operating range and better absorber performance. It should also be noted that as the mistuning level approaches $-2{\cdot}5\%$ ($\sigma = -0{\cdot}5$), the torque level at which the jump occurs approaches zero, indicating that the absorbers will jump no matter how small the applied torque is. After the jump, as will be shown later, the absorbers' motions actually add to the applied torque, thereby *increasing* vibration levels as compared to the rotor with the absorbers locked. The stability of the various steady state curves in Figure 5 are nearly as expected, with one exception. The lower branches are stable up to a torque level just prior to the jump, where the bifurcation to non-unison occurs. The middle branch is, of course, everywhere unstable, and the upper branch is everywhere stable.

Figure 6 shows a plot of the amplitude of the non-dimensional rotor acceleration, $|vv'|$, versus the applied torque level. The previous comment about the tradeoff between performance and range is clear from this figure as well, since the performance degrades as the range is increased. However, in all cases shown here (since the mistuning levels are positive in these examples), the absorbers reduce the vibration levels when compared to the system with the absorbers locked at their respective vertices (where they play the role of a simple flywheel).

It should be noted here that the jump leads to the existence of multiple unison stable responses at a given torque level. In fact, the bifurcation to non-unison leads to an even more complicated response diagram, with the possibility of several stable non-unison response branches [17].

An interesting observation is the presence of a local maximum angular acceleration of the rotor, which occurs on the lower branch of the analytical response curves. This exists just before the jump point on the simulation curves, and it has been observed that these local peak acceleration points represent the points where bifurcations to non-unison response

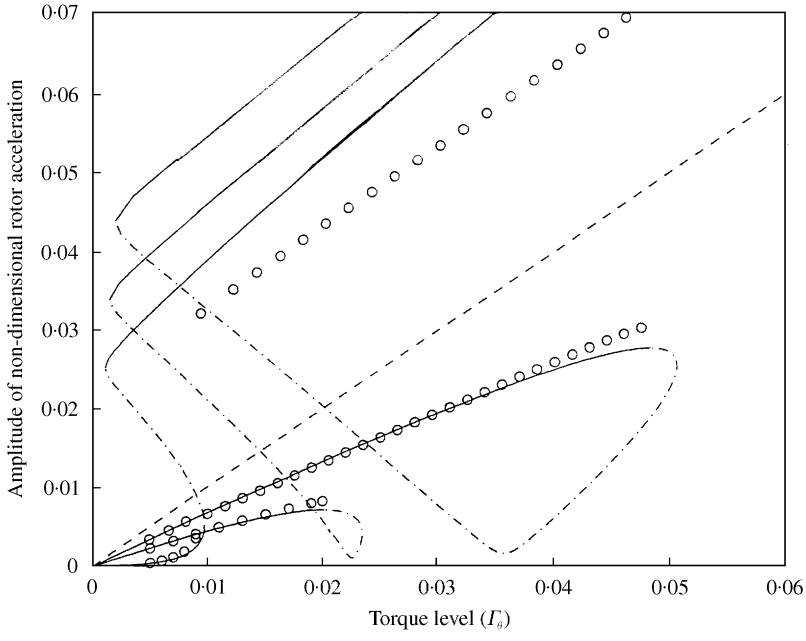

Figure 6. Amplitude of rotor acceleration versus torque level for $N = 4$ circular path CPVAs. The straight – – – line is a reference corresponding to the response with the absorbers locked at their vertices. —— lines represent stable responses predicted by the analysis, and – · – · – lines represent unstable responses. ○ ○ ○ circles indicate results from numerical simulations. Results are shown for three levels of mistuning: $\sigma = 0$ (smallest operating range), $\sigma = 0{\cdot}4$, and $1{\cdot}0$ (largest operating range).

take place. This can be shown to be the case mathematically, as follows. From equation (17) and the first of equation (19), we have

$$vv'(\theta) = \varepsilon^r[n^2 r_z \sin(n\theta + \phi_z) + \tilde{\Gamma}_\theta \sin(n\theta)] + \mathrm{O}(\varepsilon v^{r+\nu}).$$

Also, since $\tilde{\mu}_a$ is small, it is seen from equation (23) that the phase ϕ_z is close to zero or π. Before the jump, $\phi_z \approx \pi$ (as will be shown subsequently). The above equation thus becomes

$$vv'(\theta) \approx \varepsilon^r[\tilde{\Gamma}_\theta - n^2 r_z] \sin(n\theta)$$

and the rotor acceleration amplitude is thus approximated by

$$|vv'(\theta)| \approx \varepsilon^r[\tilde{\Gamma}_\theta - n^2 r_z].$$

Differentiating this result with respect to $\tilde{\Gamma}_\theta$, and making use of the second of equation (23) with $\phi_z = \pi$ (since r_z depends on $\tilde{\Gamma}_\theta$ in a non-linear manner), the following expression is obtained:

$$\frac{\mathrm{d}|vv'(\theta)|}{\mathrm{d}\tilde{\Gamma}_\theta} \approx \varepsilon^r\left[1 - \frac{n^2}{2n^2(\sigma + \frac{1}{2}) - \frac{9}{2}\gamma_0 r_z^2}\right].$$

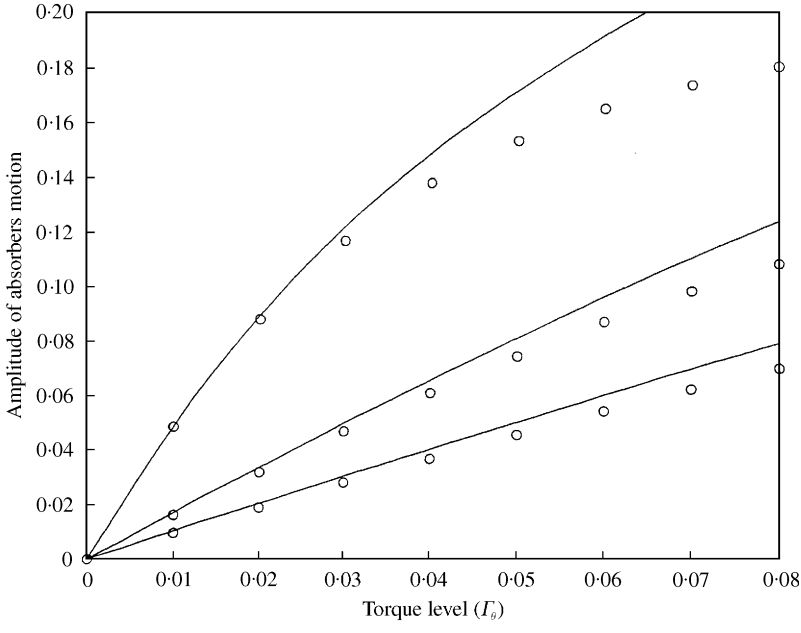

Figure 7. Absorber amplitude versus torque level for $N = 4$ cycloidal path CPVAs. —— lines are stable responses predicted from the analysis, and ○ ○ ○ circles are results from numerical simulations. The curves are for mistuning levels of: 0 (upper curve), 5 (middle curve), 10% (lower curve).

Solving this for the r_z value at which $|vv'(\theta)|$ is a maximum, i.e., where this expression is zero, one finds

$$r_z \approx \frac{2n}{3}\sqrt{\frac{\sigma}{\gamma_0}},$$

which is exactly the same as the expression for r_{zbif} given by equation (31), when the term with the damping coefficient $\tilde{\mu}_a$ is ignored. This feature of the response is not well understood, but it has been observed in preliminary experimental investigations [18].

The general response for circular paths is observed to be a unison response with a smooth increase in absorber amplitude and angular acceleration, up to a point at which the acceleration peaks and the system bifurcates to a non-unison motion. Typically, the response beyond this torque level is captured by the undesirable upper branch of the unison response. This is due to the bifurcation being sub-critical, or there being a very small basin of attraction for the post-bifurcation response [17]. In the present case with $N = 4$, the only level of mistuning where it was possible to observe the non-unison response was at 0·5%.

3.3. CYCLOIDAL PATHS

The cycloidal path offers a slightly hardening non-linearity ($\gamma_0 < 0$, as given by equation (36)), and this avoids many of the problems and shortcomings associated with circular paths. For cycloidal absorber paths, neither the bifurcation to non-unison nor jumps are present when $\sigma \geqslant 0$, as is clear from equations (37,38). Figure 7 shows theoretical and numerical simulation results for $N = 4$ absorbers with 0, 5, and 10% mistuning levels respectively.

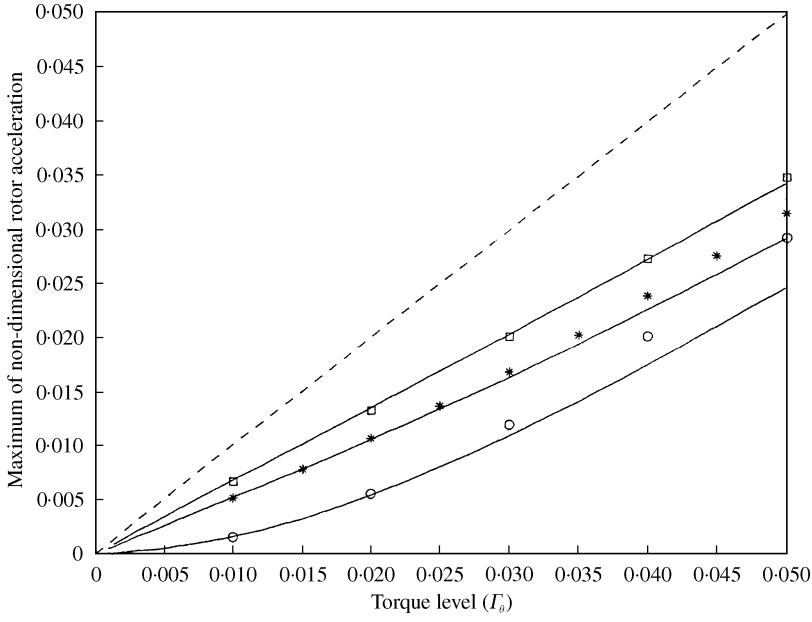

Figure 8. Amplitude of rotor acceleration $|vv'(\theta)|$ versus torque level for $N = 4$ cycloidal path absorbers, for three levels of mistuning. The – – – line is the reference with the absorbers locked. The —— curves are analytical predictions and the sets of symbols are simulation results. The lower curve and ○ ○ ○ circles are for mistuning level 0%, the middle curve and stars are for 2·5% mistuning, and the upper curve and open boxes are for 5·0% mistuning.

Similar to circular paths, increasing the mistuning levels in cycloidal paths will decrease the amplitude of the absorbers' motion for the same torque level. Figure 8 shows theoretical and numerical simulation results for the amplitude of the non-dimensional rotor angular acceleration versus torque level for $N = 4$ absorbers with 0, 2·5, and 5% mistuned cycloidal paths respectively. These results indicate that the mistuning should be kept as small as possible in order for the absorbers to effectively cancel the fluctuating torque. In this case, in contrast with circular paths, the range is not limited by a jump bifurcation.

Note that again the analytical results are quite good, but deteriorate as the absorbers' amplitude increases. It should also be noted here that the general agreement between theory and simulation is not as good as it was for circular paths. As mentioned earlier, for $\sigma < -\frac{1}{2}$, the theory predicts jumps, but this could not be found in the numerical simulations. The reason for this reduced accuracy is that cycloidal paths are much closer to epicycloidal paths where, as mentioned above, non-linearities other than the path non-linearity are also important. In any case, mistuning values of $\sigma < -\frac{1}{2}$ are not of practical importance (as described in the following section), and the theory works very well for practical levels of mistuning.

An interesting range of mistuning that deserves further mention is $-\frac{1}{2} < \sigma < 0$. For mistuning levels in this range, the theory predicts an amplitude range where the unison response is unstable. This range can be found using equation (37). For cycloids, it was possible to numerically find some stable steady state non-unison responses in these ranges. Table 1 shows the theoretical ranges of absorber amplitudes and torque levels at which the unison response is unstable for a system with $N = 4$ absorbers, for different mistuning levels. The two absorber amplitudes and torque levels correspond to the lower and upper bounds of this unstable region. Figure 9 shows the numerically simulated steady state absorber responses for $\sigma = -0{\cdot}2$ for a set of torque levels that run through the unstable

TABLE 1

Theoretical ranges of absorber amplitudes and torque levels at which non-unison motions exist for $N = 4$ absorbers with cycloidal paths

Mistuning (σ)	r_{z1}	r_{z2}	$\Gamma_{\theta 1}$	$\Gamma_{\theta 2}$
−0·10	0·30	0·50	0·012	0·022
−0·20	0·42	0·71	0·014	0·032
−0·30	0·51	0·88	0·014	0·039
−0·40	0·58	1·01	0·012	0·045

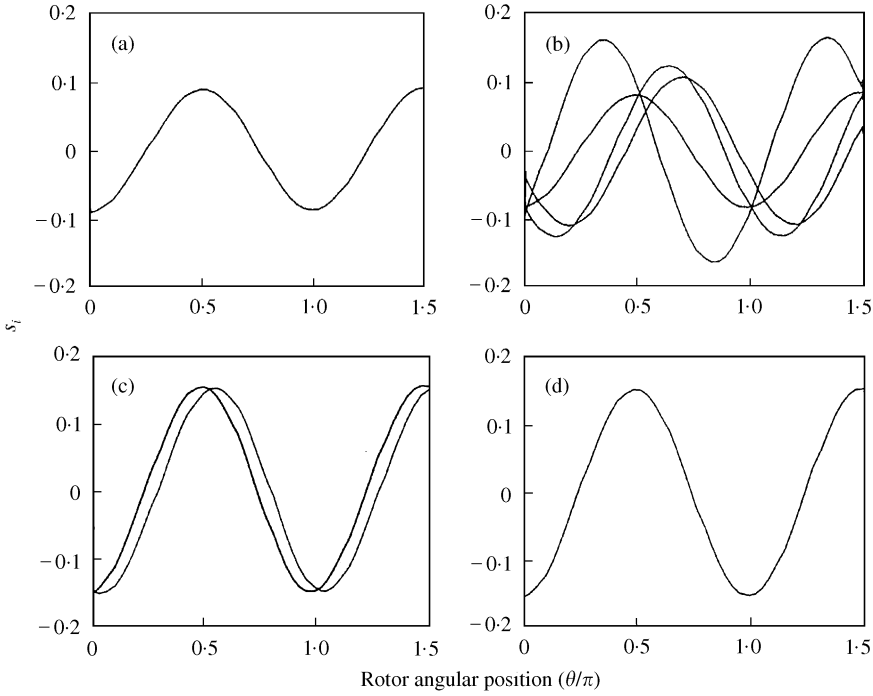

Figure 9. Numerical simulations of cycloidal path absorbers' responses for $\sigma = -0{\cdot}2$, $N = 4$ and four different levels of torque: (a) $\Gamma_\theta = 0{\cdot}0125$, (b) 0·014, (c) 0·032 and (d) 0·0335.

range. There are evidently a number of bifurcations in this range, leading to a variety of possible responses. For this reason, and other reasons to be outlined below, negative mistuning should be avoided for any path type.

3.4. COMMENTS ON THE ABSORBER SYSTEM PERFORMANCE

In order to determine how the performance of the absorbers is affected by the level of mistuning, one can consider equation (23), along with the fact that the absorber damping $\tilde{\mu}_a$ is small. It can be seen that the absorbers' steady state phase angle ϕ_z is close to either 0 or π.

For paths with $\gamma_0 > 0$, for example circular paths, if $\sigma > -\frac{1}{2}$ and the absorbers' amplitude of vibration is small enough, which is the case here, then ϕ_z is close to π. Then, from

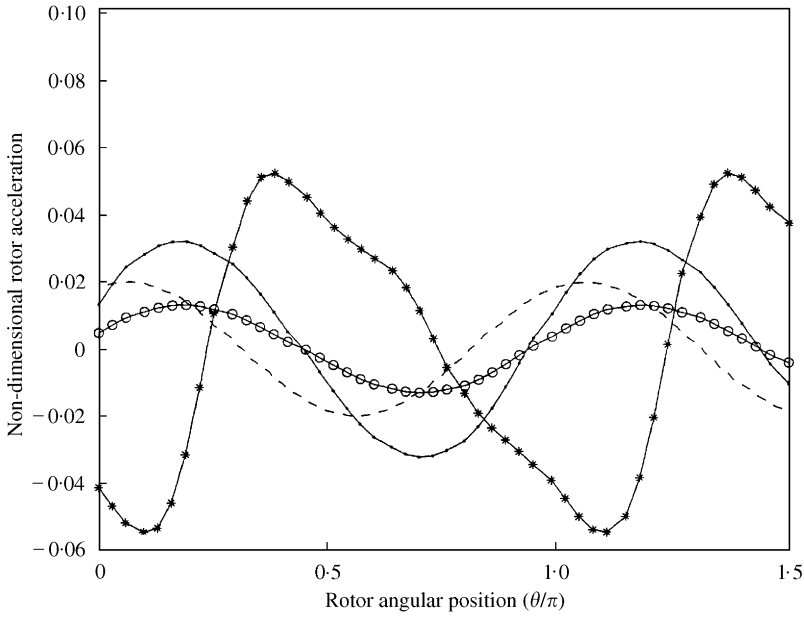

Figure 10. Numerical simulation of the steady state rotor angular acceleration, $vv'(\theta)$, versus θ for $\Gamma_\theta = 0{\cdot}02$ for $N = 4$ mistuned circular path absorbers. The – – – line is for the absorbers locked, the — line with $\cdots$ is for $-5{\cdot}0\%$ mistuning, the —— line with $***$ is for 5·0% mistuning on the upper branch of the response curve, and the —— line with $\bigcirc\bigcirc\bigcirc$ circles is for 5·0% mistuning on the lower branch of the response curve.

equation (17), along with equation (19), one concludes that the absorbers are producing a torque which is opposite in phase to the applied torque. If the absorbers' amplitude of vibration is increased, say, by increasing the applied torque level, then it will reach a value where $\cos(\phi_z)$ will jump from near (-1) to near $(+1)$. This corresponds to the jump beyond which the system operates on the upper part of the response curve. Here the motions of the absorbers are in phase with the applied torque, thereby increasing torsional vibration levels. An example of this is seen in Figure 6, wherein the upper stable branch of the acceleration response curves are above the reference line. For $\sigma \leqslant -\frac{1}{2}$, $\cos(\phi_z)$ is always near $(+1)$ and the absorbers always add to the applied torque. These facts are demonstrated by the simulation results for $N = 4$ absorbers, as shown in Figure 10. This figure shows the non-dimensional rotor angular acceleration, $vv'(\theta)$, versus rotor angle for steady state responses on the lower and the upper portions of the response curve for $+5\%$ mistuning levels and a torque amplitude of 0·02. It also shows $vv'(\theta)$ for the same torque level but with a mistuning level of -5%, and for the absorbers locked at their vertices. Note that the absorbers actually increase the vibration level when on the upper branch of the response curve and for the negative mistuning level.

For paths with $\gamma_0 < 0$, for example cycloidal paths, when $\sigma \leqslant -\frac{1}{2}$, equation (23) indicates that ϕ_z is near 0. This implies that the absorbers are always adding torsional vibrations to the rotor. For $\sigma > -\frac{1}{2}$, then ϕ_z is close to π and the absorbers are reducing the rotor torsional vibrations, as long as they move in unison. However, for $-\frac{1}{2} < \sigma < 0$ there are ranges of applied torques where non-unison motions exist, and one cannot conclude that the absorbers are working properly in (or near) these torque ranges. For $\sigma \geqslant 0$, the absorbers reduce torsional vibrations at all torque levels. This is because, for $\sigma \geqslant 0$, neither bifurcations to non-unison nor jumps are present. Figure 11 shows numerical simulation results for the non-dimensional rotor angular acceleration of $N = 4$ cycloidal path

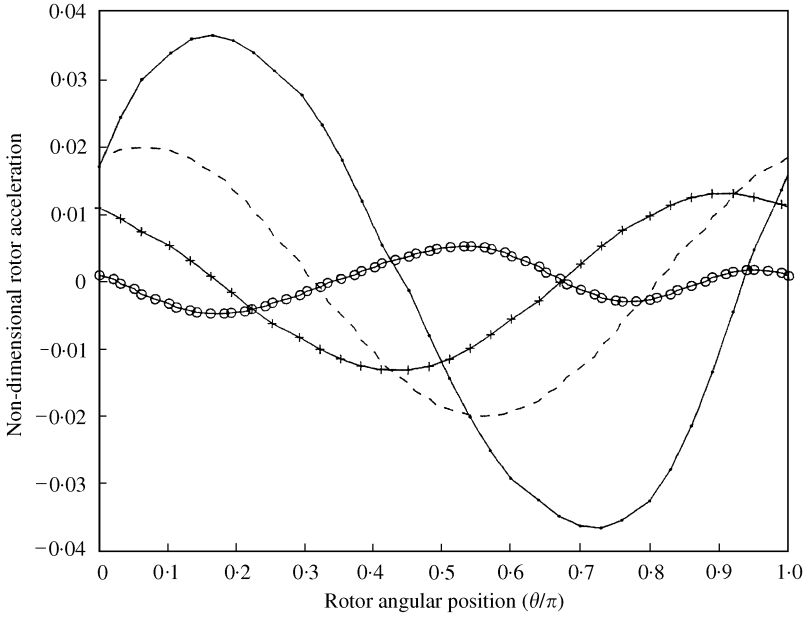

Figure 11. Numerical simulation of the steady state rotor angular acceleration, $vv'(\theta)$, versus θ for $\Gamma_\theta = 0{\cdot}02$ for $N = 4$ mistuned cycloidal path absorbers. The − − − line is for the absorbers locked, the —— line with ⋯ is for $-5{\cdot}0\%$ mistuning, the —— line with + + + is for $5{\cdot}0\%$ mistuning, and the —— line with ○ ○ ○ circles is for 0% mistuning.

absorbers with 0, 5, and -5% mistuning levels, subjected to a torque of amplitude 0·02. These effects are clearly demonstrated here.

4. SUMMARY AND CONCLUSIONS

The following points summarize the findings of this study:

For paths ranging from circular up to, but not including, epicycloidal paths, that is, for $0 \leqslant \lambda < \lambda_e$.

- There are positive mistuning levels below which no bifurcations to non-unison are present. These levels are usually very small and are parameter dependent.
- Jumps are always present for paths with mistunings $\sigma > -\frac{1}{2}$.
- Paths other than circular ones do not have significant benefits over the easily manufactured circular path.
- For paths with $\sigma > -\frac{1}{2}$, the absorbers reduce torsional vibrations for absorber responses that are on the lower portions of the response curves, but they increase torsional vibration for responses on the upper portions of the response curves.

For paths ranging from, but not including, epicycloidal paths up to cycloidal paths, that is, for $\lambda_e < \lambda \leqslant 1$.

- Neither bifurcations to non-unison nor jumps are present for perfectly tuned and positively mistuned paths, that is, for $\sigma \geqslant 0$.
- For negatively mistuned paths, $\sigma < 0$, there are torque ranges where non-unison motions exist.

- The analysis presented predicts jumps for paths with $\sigma < -\frac{1}{2}$, but these are not found in the numerical simulations.[§]

For all paths considered.

- As the mistuning levels are positive and increased, the bifurcation to non-unison and the jump points, if they exist, are pushed out to higher torque levels, and they approach each other, thus resulting in increased torque operating ranges.
- When the operating ranges are increased by increasing the mistuning levels, the effectiveness of the absorber system, in terms of reducing rotor torsional vibrations, is reduced.
- With $\sigma \leqslant -\frac{1}{2}$, the absorbers actually increase, rather than reduce, the levels of torsional vibration.

In light of these observations, one can conclude that for any type of absorber path, when the absorber amplitudes are kept very small it is best not to have any mistuning, i.e., perfectly tuned paths are the best choice. However, if one wants to increase the operating range, positive mistuning levels should be selected, keeping in mind that the absorbers' performance will be reduced. Negative mistuning levels should always be avoided.

When the performance of absorber systems with circular and cycloidal paths are compared, it is concluded that absorbers with cycloidal paths are preferred because they do not undergo jump bifurcations nor bifurcations to non-unison steady state responses, thereby resulting in much larger working ranges. The lack of instability of the unison response implies that only one steady state response exists at each torque level, and this response is equivalent to that predicted by using a model with a single absorber mass, thus making design analysis much easier.

In addition, as will be described in a forthcoming paper, one should always use a small amount of positive mistuning for any absorber path, in order to avoid vibration localization that can arise from slight differences among the absorbers [17].

REFERENCES

1. C. F. Taylor 1985 *The Internal Combustion Engine in Theory and Practice*. Cambridge, Massachusetts: The MIT Press.
2. O'Connor 1947 *Society of Automotive Engineering Quarterly Transactions* **1**, 87. The viscous torsional vibration damper.
3. W. Ker Wilson 1968 *Practical Solutions of Torsional Vibration Problems*, Vol. IV. London: Chapman & Hall Ltd; chapter XXX.
4. Pierce 1945 *Transactions of Society of Automotive Engineering* **53**, 480. Rubber mounted dampers, examples of application.
5. B. C. Carter 1929 *British Patent No.* 337, 446.
6. J. F. Madden 1980 *United States Patent No.* 4218187. Constant frequency bifilar vibration absorber.
7. M. Cook 1994 *Car Craft* August, p. 75. Absolute absorption.
8. H. H. Denman 1992 *Journal of Sound and Vibration* **159**, 251–277. Tautochronic bifilar pendulum torsion absorbers for reciprocating engines.
9. V. J. Borowski, H. H. Denman, D. L. Cronin, S. Shaw, J. P. Hanisco, L. T. Brooks, D. A. Milulec, W. B. Crum and M. P. Anderson 1991 *The Engineering Society for Advanced Mobility Land, Sea, Air, and Space*. SAE Technical Paper Series 911876. Reducing vibration of reciprocating engines with crankshaft pendulum vibration absorbers.

[§]This may be due to the fact that these paths are near the epicycloid and have a relatively weak path non-linearity, in which case other non-linearities, which have been scaled out of the present analysis, may come into play.

10. C. T. LEE and S. W. SHAW 1995 *American Society of Mechanical Engineers Design Engineering Technical Conference*, Vol. DE-Vol. 84-1, Vol. 3-Part A, 487–492. Torsional vibration reduction in internal combustion engines using centrifugal pendulums.
11. C. T. LEE and S. W. SHAW 1994 *Nonlinear and Stochastic Dynamics*, *American Society of Mechanical Engineers* Volume AMD-Vol. 192/DE-Vol. 78, 91–98. A comparative study of nonlinear centrifugal pendulum vibration absorbers.
12. S. W. SHAW, V. GARG and C. P. CHAO 1997 *SAE Noise and Vibration Conference and Exposition.* Attenuation of engine torsional vibrations using tuned pendulum absorbers.
13. C. P. CHAO, C. T. LEE and S. W. SHAW 1996 *American Society of Mechanical Engineers Journal of Applied Mechanics* **64**, 149–156. Stability of the unison response for a rotating system with multiple tautochronic pendulum vibration absorbers.
14. D. E. NEWLAND 1964 *American Society of Mechanical Engineers Journal of Engineering for Industry* **86**, 257–263. Nonlinear aspects of the performance of centrifugal pendulum vibration absorbers.
15. C. P. CHAO, C. T. LEE and S. W. SHAW 1997 *Journal of Sound and Vibration* **204**, 769–794. Non-unison dynamics of multiple centrifugal pendulum vibration absorbers.
16. M. GOLUBITSKY, I. STEWART and D. G. SCHAEFFER 1988 *Singularities and Groups in Bifurcation Theory*, Vol. II. New York: Springer-Verlag.
17. A. ALSUWAYIAN 1999 *Ph.D. Dissertation*, *Department of Mechanical Engineering*, *Michigan State University*, *East Lansing*, *MI*, *U.S.A.* Dynamic stability and localization of systems of vibration absorbers.
18. A. G. HADDOW and S. W. SHAW 2001 *Proceedings of the* 18*th Biennial Conference on Vibration and Noise*, Paper DETC 2001/VIB-21754. An experimental study of torsional vibration absorbers.

APPENDIX A: NOMENCLATURE

a_i	amplitude of the ith absorber response
$\bar{a}_i$	averaged version of a_i
A	Jacobian for averaged version of unison response
$A1$	2×2 block component of A
$A1_{ij}$	elements of $A1$
$A2$	2×2 block component of A
$A2_{ij}$	elements of $A2$
$b_i = I_i/J$	inertia ratio for the ith absorber
$b_0 = I_0/J$	inertia ratio when the absorbers are identical
c_{ai}	equivalent viscous damping constant for the ith absorber
c_0	equivalent viscous damping constant for the rotor
f_i	function defined during averaging
$\tilde{g}_i(s_i)$	non-dimensional version of $\tilde{G}_i(S_i)$
$\tilde{G}_i(S_i)$	path function for ith absorber
i	index for absorber identification
$I_i = m_i R_{i0}^2$	moment of inertia of the ith absorber at its vertex
$I_0 = m R_0^2$	I_i's when the absorbers are identical
J	moment of inertia of the rotor
l	scaling order parameter
m_i	mass of ith absorber
m	mass of each absorber when they are identical
$m_0 = Nm$	total mass of all absorbers when they are identical
n	order of the applied torque
$\tilde{n}_i$	tuning order for the ith absorber
N	number of absorbers
p	scaling order parameter
q	scaling order parameter
r	scaling order parameter
r_z	averaged amplitude of absorbers' responses when moving in unison
r_z'	rate of averaged, unison amplitude change with respect to θ
r_{zbif}	value of r_z when bifurcation to non-unison occurs
r_{zj}	value of r_z when jump bifurcation occurs

$r_i(s_i)$	non-dimensional version of $R_i(S_i)$
$R_i(S_i)$	distance from center of rotation to m_i at S_i
$R_{i0} = R_i(0)$	distance from center of rotation to m_i at $S_i = 0$
$R_0 = R(0)$	R_{i0} when the absorbers are identical
s_i	non-dimensional position of ith absorber along its path
s_i'	non-dimensional path speed of ith absorber with respect to θ
s_i''	non-dimensional path acceleration of ith absorber with respect to θ
S_i	position of ith absorber along its path
$\dot{S}_i$	path speed of ith absorber
$\ddot{S}_i$	path acceleration of ith absorber
T_0	constant component of the torque acting on the rotor
$T(\theta)$	fluctuating component of the torque acting on the rotor
$v = \dot{\theta}/\Omega$	non-dimensional rotor speed
$v' = \mathrm{d}v/\mathrm{d}\theta$	non-dimensional rotor acceleration as measured by the rotor angle
w	scaling order parameter
$X_i(S_i) = R_i^2(S_i)$	square of the distance from center of rotation to m_i at S_i
$x_i(s_i)$	non-dimensional version of $X_i(S_i)$
z_i	scaled version of s_i
z_i'	scaled version of s_i'
z_i''	scaled version of s_i''
ε	scaling parameter
ϕ_i	phase of ith absorber response
$\bar{\phi}_i$	averaged version of ϕ_i
ϕ_z	averaged phase of absorbers' response when moving in unison
ϕ_z'	rate of averaged, unison phase change with respect to θ
γ_i	non-linear parameter for the expanded form the ith path
γ_0	γ_i for perfectly tuned, identical paths
Γ_0	non-dimensional constant torque
$\tilde{\Gamma}_0$	scaled version of Γ_0
$\Gamma(\theta)$	non-dimensional fluctuating torque
$\tilde{\Gamma}(\theta)$	scaled version of $\Gamma(\theta)$
λ	non-linear path parameter
$\lambda_e = \sqrt{\tilde{n}^2/(\tilde{n}^2+1)}$	non-linear path parameter for the tautochronic epicycloidal path
μ_{ai}	non-dimensional damping coefficient for the ith absorber
μ_0	non-dimensional damping coefficient for the rotor
$\tilde{\mu}_a$	scaled version of μ_a for identical absorbers
$\tilde{\mu}_0$	scaled version of μ_0
ν	scaling order parameter
Ω	mean rotor speed
θ	rotor angle
$\dot{\theta}$	rotor angular speed
$\ddot{\theta}$	rotor angular acceleration
ρ_i	the local radius of curvature of the ith path
ρ_{i0}	the local radius of curvature of the ith path at $S_i = 0$
σ_i	mistuning parameter for the ith absorber
σ	mistuning parameter when absorbers are identical
$()'$	differentiation with respect to θ
$\dot{()}$	differentiation with respect to time